International Journal of Nanomedicine

Dovepress
open access to scientific and medical research

Open Access Full Text Article

ORIGINAL RESEARCH

pH-sensitive Au–BSA–DOX–FA nanocomposites for combined CT imaging and targeted drug delivery

This article was published in the following Dove Press journal:
International Journal of Nanomedicine
6 April 2017
Number of times this article has been viewed

He Huang[1]
Da-Peng Yang[2]
Minghuan Liu[2]
Xiangsheng Wang[1]
Zhiyong Zhang[1]
Guangdong Zhou[1]
Wei Liu[1]
Yilin Cao[1]
Wen Jie Zhang[1]
Xiansong Wang[1]

[1]Department of Plastic and Reconstructive Surgery, Shanghai Ninth People's Hospital, Shanghai Jiao Tong University School of Medicine, Shanghai Key Laboratory of Tissue Engineering, National Tissue Engineering Center of China, Shanghai, [2]College of Chemical Engineering and Materials Science, Quanzhou Normal University, Quanzhou, People's Republic of China

Abstract: Albumin-based nanoparticles (NPs) as a drug delivery system have attracted much attention owing to their nontoxicity, non-immunogenicity, great stability and ability to bind to many therapeutic drugs. Herein, bovine serum albumin (BSA) was utilized as a template to prepare Au–BSA core/shell NPs. The outer layer BSA was subsequently conjugated with *cis*-aconityl doxorubicin (DOX) and folic acid (FA) to create Au–BSA–DOX–FA nanocomposites. A list of characterizations was undertaken to identify the successful conjugation of drug molecules and targeted agents. In vitro cytotoxicity using a cell counting kit-8 (CCK-8) assay indicated that Au–BSA NPs did not display obvious cytotoxicity to MGC-803 and GES-1 cells in the concentration range of 0–100 μg/mL, which can therefore be used as a safe drug delivery carrier. Furthermore, compared with free DOX, Au–BSA–DOX–FA nanocomposites exhibited a pH-sensitive drug release ability and superior antitumor activity in a drug concentration-dependent manner. In vivo computed tomography (CT) imaging experiments showed that Au–BSA–DOX–FA nanocomposites could be used as an efficient and durable CT contrast agent for targeted CT imaging of the folate receptor (FR) overexpressed in cancer tissues. In vivo antitumor experiments demonstrated that Au–BSA–DOX–FA nanocomposites have selective antitumor activity effects on FR-overexpressing tumors and no adverse effects on normal tissues and organs. In conclusion, the Au–BSA–DOX–FA nanocomposite exhibits selective targeting activity, X-ray attenuation activity and pH-sensitive drug release activity. Therefore, it can enhance CT imaging and improve the targeting therapeutic efficacy of FR-overexpressing gastric cancers. Our findings suggest that Au–BSA–DOX–FA nanocomposite is a novel drug delivery carrier and a promising candidate for cancer theranostic applications.

Keywords: gold nanoparticles, bovine serum albumin, CT imaging, drug delivery, theranostics

Introduction

Nanomedicine provides an unprecedented opportunity to improve significantly the way in which many diseases are treated,[1] in part because of the rapid development of nanomaterials. Among well-known nanomaterials, gold nanoparticles (GNPs) have gained considerable attention owing to their excellent biocompatibility,[2] inert reactivity, good photostability, facile synthesis, non-cytotoxicity[3] and solubility.[2,4] To date, GNPs have been widely studied in various biomedical applications, including bioimaging, single molecule tracking, biosensing, drug delivery[5–9] and as contrast-enhancing agents in X-ray and computed tomography (CT) applications.[10–14] Cancer is considered to be a worldwide mortal disease, which has become a major public concern. Early findings and treatments are still the focus of research efforts to overcome cancer.

Correspondence: Wen Jie Zhang; Xiansong Wang
Department of Plastic and Reconstructive Surgery, Shanghai Ninth People's Hospital, Shanghai Jiao Tong University School of Medicine, Shanghai Key Laboratory of Tissue Engineering, National Tissue Engineering Center of China, 639 Zhi Zao Ju Road, Shanghai 200011, People's Republic of China
Tel +86 21 2327 1699
Fax +86 21 5307 8128
Email wenjieboshi@aliyun.com; vincentuis@126.com

submit your manuscript | www.dovepress.com
Dovepress
http://dx.doi.org/10.2147/IJN.S128270

Thus, it is highly desirable to develop novel functionalized GNPs, which could not only detect cancer cells but also deliver the drugs within the cancerous targets.

Inspired by biomineralization, protein-based synthesis was explored for the production of nanoparticles (NPs) in an eco-friendly manner.[15] The resulting products are often coated by a layer of protein molecules and are beneficial for biomedical applications. Bovine serum albumin (BSA) is often used as a template to synthesize nanocomposites, including Au–BSA NPs/clusters, which has been further explored for tumor imaging applications and targeted cancer therapy.

For example, Chen et al used BSA as a template to synthesize ultra-small Au nanoclusters. To further form Au–FA–MPA nanocomposites, folic acid (FA) and MPA (a near-infrared fluorescent dye) were adhered to the surface of BSA. The nanoprobe displayed low toxicity against tumor cells in vivo and in vitro, a bright fluorescence signal and an outstanding tumor targeting ability due to folate receptor (FR)-mediated uptake.[16] In another research, Murawala et al synthesized Au NPs capped with BSA molecules in situ. The Au–BSA NPs had superior stability against different mediums and were used as an effective anticancer drug carrier to load methotrexate into MCF-7 breast cancer cells as a chemotherapy treatment.[17] Ding and Tian[18] used BSA as a substrate to fabricate FA–fluorescein isothiocyanate@AuNC as a ratiometric fluorescence biosensor for specific bioimaging and biosensing in cancer cells. Therefore, BSA-based GNPs represent an attractive strategy to fabricate a drug delivery carrier. Compared with other types of substrates, BSA had the ability to bind many drug moieties at a high capacity due to the high number of potential drug binding sites present in this protein.[19,20]

Tumor tissue is usually reported to be acidic because of the deprivation of nutrients and an insufficient removal of metabolic waste products, mainly lactic acid. A useful method to facilitate drug delivery is the incorporation of acid-sensitive bonds between the polymer and drug, ensuring the successful release of encapsulated drug in the tumor.[9,21] Among the most useful acid-labile linkers, *cis*-aconityl acid is frequently used when trying to design an ideal drug delivery system.[22] Compared with a nonconjugated system, a drug in this delivery system shows enhanced antitumor activity and a relative reduction in nonspecific toxicity to normal tissue.[22] As conventional anticancer drugs usually have severe toxicity, low selectivity and many adverse effects, it is necessary to combine them with some candidate ligands to deliver selectively anticancer drugs to tumor cells. Xiao et al[8] reported cyclic arginine–glycine–aspartic acid (cRGD) peptide-conjugated gold nanorods (GNRs) for targeted anticancer drug delivery and imaging of tumors. As one of the targeting agents, cRGD peptide actually reduced the tumor accumulation of the GNRs two- to three-fold, which may reduce antitumor efficiency. Among targeting agents, FA has been extensively used as a selective drug target. Indeed, recent reports suggest that folate-conjugated NPs can decrease the toxicity of anticancer drugs and significantly improve the antitumor effects.[16,22]

CT is a molecular imaging technology[23,24] that is often used to diagnose cancer.[25,26] X-ray contrast agents are often utilized to improve the sensitivity and specificity of CT in detecting cancer.[11,13,27] Conventionally used small molecular iodinated CT contrast agents have a number of drawbacks, including potential renal toxicity, a brief time spent in the circulation and poor target specificity.[28,29] It is likely that the shortcomings mentioned earlier can be overcome by developing new types of non-iodinated CT contrast agents. For higher atomic numbers and electron densities greater than iodine, gold can be usefully incorporated into a new generation of contrast agents. One useful property of gold in this role is its ability strongly to attenuate X-rays, making gold an ideal component for incorporation into contrast agents.[30–32] Furthermore, surfaces of Au NPs functionalized with tumor-specific biomarkers can also be used to target specifically cancerous cells in vitro or tumors in vivo.[33–37] Recently, Du et al[22] demonstrated that FA–BSA–CAD prodrug selectively targeted tumor cells and tissues, with associated reduction in nonspecific toxicity to the normal cells. Based on these reports, we designed and synthesized Au–BSA–doxorubicin (DOX)–FA nanocomposites. Au–BSA–DOX–FA nanocomposites can serve as CT contrast agent for FA-positive tumors compared to FA–BSA–CAD prodrug.

In the present study, crystalline Au was initially trapped within BSA and then successively conjugated with *cis*-aconitic anhydride-doxorubicin (*cis*-DOX) and FA to create Au–BSA–DOX–FA nanocomposites (Figure 1).

In these nanocomposites, Au offered its brilliant X-ray attenuation property, while BSA offered a template and free amino groups to couple DOX as chemotherapeutic agents and FA that can specifically bind to the aberrantly overexpressed FR in malignant tumor cells.[38–40] After loading identification of FA and DOX, validation of the control release of DOX and its characterization, the as-synthesized nanocomposites, were submitted to explore their potential in CT diagnostics and targeting therapy of FR-overexpressing gastric cancer. The findings suggested that Au–BSA–DOX–FA nanocomposite

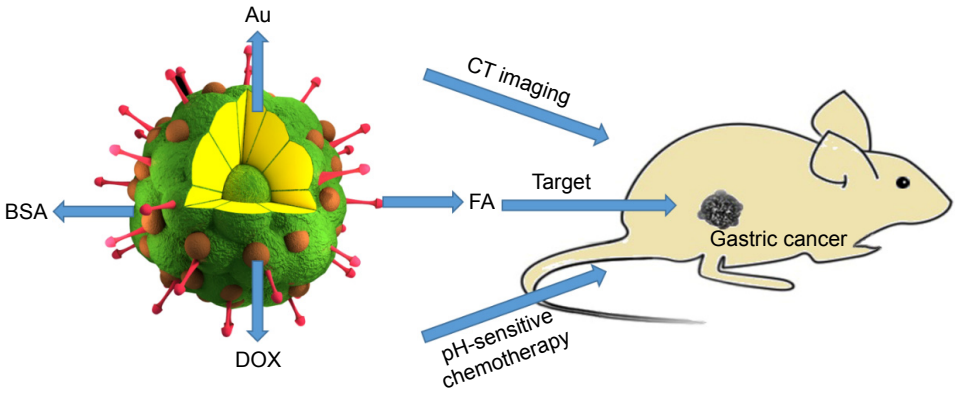

Figure 1 Schematic diagram of an Au–BSA–DOX–FA nanocomposite model and multifunction in CT imaging and targeting therapy in FR-overexpressing gastric cancer xenografted mice.
Abbreviations: BSA, bovine serum albumin; DOX, doxorubicin; FA, folic acid; CT, computed tomography; FR, folate receptor.

can act as a novel drug delivery carrier, with promising uses in cancer theranostic applications.

Materials and methods

Characterization and fabrication of Au–BSA–DOX–FA nanocomposites

Fabrication of Au–BSA NPs

Freshly prepared aqua regia solution was used to thoroughly clean glassware, followed by extensive rinsing in distilled water before use. A stock of 10 mL of 5 mg/mL BSA was prepared by dissolving BSA in Millipore water. A total of 1 mL of chloroauric acid solution (10 mM) was prepared by adding $HAuCl_4$ to Millipore water. Then, the $HAuCl_4$ solution was mixed with BSA followed by the addition of 20 mg ascorbic acid during magnetic stirring at room temperature for 30 min. The previously formed yellow solution became colorless and finally was converted to purple blue, indicating the formation of Au NPs. It was established that the aqueous solution of Au–BSA NPs was stable for >1 month when stored at room temperature.

Conjugation of DOX with an Au–BSA NP (Au–BSA–DOX)

In order to conjugate DOX with Au–BSA, a *cis*-aconityl bond was initially introduced onto DOX according to a method reported in the literature.[22] In brief, 5 mg of *cis*-aconitic anhydride was dissolved in 200 µL of 1,4-dioxane and slowly pipetted into a cooled DOX solution (7 mg DOX in 4 mL of ultrapure water) during vigorous stirring, and subsequently, the pH was rapidly adjusted to pH 9.0 by the addition of 0.5 M NaOH solution. Then, the reaction vessel was placed in a water bath containing ice for 20 min. Then, the pH was adjusted to pH 7.0 by the addition of HCl (1.0 M) under stirring for another 30 min until a precipitate of *cis*-DOX was produced. The mixture was centrifuged at 8,000 rpm for 10 min, and then, the precipitate was isolated. Pellet structure was determined using liquid chromatography–mass spectrometry (LC-MS) before being dissolved in 3 mL of ultrapure water containing 7 mg of 1- Ethyl-3-(3-dimethylaminopropyl) carbodiimide and 3 mg of N-Hydroxysuccinimide (NHS). The solution was stirred for 4 h in light-free conditions at the ambient room temperature. Then, Au–BSA NPs (2 mL, 50 mg/mL) in ultrapure water was added, and the solution was stirred for 16 h under the same conditions described earlier (vide supra). Free BSA and DOX were separated from the product Au–BSA–DOX, after filtration through a Sephadex G-25 column.

Coupling of FA with Au–BSA–DOX

Conjugation of FA with Au–BSA–DOX (through amide bond formation) was carried out according to the method reported in the literature.[22] Briefly, 2 mg of NHS and 3 mg of EDCl were added to the FA/dimethyl sulfoxide (DMSO; 5 mg/mL) solution, which was then mechanically stirred for 4 h at ambient room temperature under light-free conditions. Then, the mixture was slowly merged with the Au–BSA–DOX solution containing 3 mL of 50 mg/mL in ultrapure water and the solution agitated at ambient room temperature under light-free conditions for 10 h. Subsequently, the mixture solution was separated from the free FA and purified using a Sephadex G-25 filtration system (defined as Au–BSA–DOX–FA).

Characterization of the Au–BSA–DOX–FA nanocomposite

The as-prepared Au–BSA–DOX–FA nanocomposites' morphology and sizes were determined using transmission electron microscopy (TEM; Tecnai G2 spirit Biotwin, [FEI,

Hillsboro, Oregon, USA]) and high-resolution transmission electron microscopy at accelerating voltages of 10 and 200 kV, respectively. The hydrodynamic diameter and size distribution of the GNPs were determined by dynamic light scattering (DLS) using a standard laboratory-built light scattering spectrometer (Nicomp 380 ZLS; Particle Sizing Systems, Port Richey, FL, USA). X-ray diffraction measurements were made using a AXD D8 instrument (40 kV, 40 mA; Bruker, Karlsruhe, Germany) with Cu-K alpha radiation (λ =1.5406 Å). A spectrometer (Equinox 55 FTIR, wavelength range: 500–4,000 cm^{-1}; Bruker) was employed to record Fourier transform infrared spectrophotometer measurements. The absorption spectrum of Au–BSA–DOX–FA nanocomposites was detected using a DU-640 UV–vis spectrophotometer (Beckman Coulter, Brea, CA, USA) operated in the range of 200–800 nm at different time intervals to determine the different conjugators in the as-prepared products.

Validation of controlled release of DOX from Au–BSA–DOX–FA

In vitro release profiles of DOX from Au–BSA–DOX–FA nanocomposites were carried out by changing the pH of the nanocomposites. Briefly, Au–BSA–DOX–FA nanocomposites (1 mL) with DOX (30 µg) attached were first placed in a dialysis tube. Subsequently, they were placed in plastic tubes containing 10 mL of saline-sodium citrate (SSC) and NaOH solution at different pH values (pH 5.0, 6.0, 7.0, 8.0, 9.0 and 10.0). Then, the tubes were shaken horizontally (50 rpm at 37°C). The medium was replaced with fresh medium at predetermined time intervals and then analyzed using ultraviolet (UV)–vis spectrometry. The amount of released DOX was quantified by reference to a standard curve.

In vitro cell studies

Cell culture

Human gastric mucosa cells (GES-1) and a gastric cancer cell line (MGC-803) were obtained from the Cell Bank, Chinese Academy of Sciences, and cultured in Dulbecco's Modified Eagle's Medium (DMEM) medium containing 1% antibiotics (streptomycin and penicillin) and 10% fetal bovine serum (FBS) at 37°C in a humid environment gassed with 5% CO_2.

Expression of FR in MGC-803 and GES-1 cells

Expression levels of FR in MGC-803 and GES-1 cells were assessed by quantitative reverse transcription polymerase chain reaction (qRT-PCR). RNA was extracted from freshly isolated cells using an RNeasy Mini Kit and transformed into cDNA using Superscript III Reverse Transcriptase. Then, 1.0 µL aliquots of cDNA were used for qRT-PCR amplification using a Power SYBR Green PCR Master Mix (Thermo Fisher Scientific, Waltham, MA, USA) in a real-time cycler (Stratagene Mx3000 PTM QPCR System; Agilent Technologies, Santa Clara, CA, USA). To amplify FR, the primers used were 5′-GAA ATC CCT GCC CTG TTC A-3′ (sense) and 5′-TGC GGT GTC TGG TTT ATT C-3′ (antisense).

Cytotoxicity and antitumor activity in vitro

To identify the potential cytotoxicity of Au–BSA in normal and cancer cells, a cell counting kit-8 (CCK-8; Dojindo, Kumamoto, Japan) was employed. The effects of Au–BSA–DOX–FA nanocomposites and free DOX on different cell lines were also investigated. GES-1 and MGC-803 cells were seeded into 96-well plates (5,000 cells/well) and incubated overnight. Regarding the cytotoxicity assay, Au–BSA at various concentrations (0, 1.56, 3.13, 6.25, 12.5, 25.0, 50.0 and 100 µg/mL) was added. For effect comparisons, these cells were treated with Au–BSA–DOX–FA nanocomposites bearing different concentrations of DOX or various doses of free DOX (46.9, 93.8, 188, 375, 750 and 1,500 ng/mL). After 48 h, the cells were washed three times with phosphate-buffered saline (PBS) at pH 7.0 and CCK-8 reagent was added (10 µL/100 µL medium); the cells were subsequently incubated for 2 h at 37°C. The optical density of the cells at 450 nm was measured and used to evaluate the viability of cells. Each experiment was performed in three parallel wells and repeated three times.

In vivo studies

Animals and gastric cancer xenograft model

The Guidance Suggestions for the Care and Use of Laboratory Animals in China were strictly adhered to. Male BALB/c-nu nude mice weighing 20–24 g, obtained from the Shanghai Chuansha Experimental Animal Raising Farm (Shanghai, China), were housed under aseptic conditions in a small animal isolator in groups of five in standard cages. The animals were exposed to a 12 h light/dark cycle, with ad libitum water and chow. All animals were acclimated to the animal facility for at least 7 days before experiments commenced. The study protocols were approved by the Animal Care and Experiment Committee of Shanghai Jiao Tong University School of Medicine.

Human gastric cancer MGC-803 cells, in the logarithmic phase of division, were harvested and resuspended in PBS. Then, cancer cells were subcutaneously implanted into athymic nude mice (5×10^6 cells/mouse). When the tumor

nodules grew to a volume of ~0.5×0.5×0.5 cm^3, the mice were used to investigate histotoxicity and antitumor activity. When the tumor nodules in the gastric cancer xenograft mice reached a volume of ~0.8×1.0×1.0 cm^3, after ~5 weeks of postimplantation, mice were submitted to analysis for CT imaging.

CT imaging of FR-overexpressing gastric cancer in vivo

The targeting ability of as-synthesized NPs was evaluated in vivo using a Brilliance 64-slice CT scanner (Royal Philips, Amsterdam, The Netherlands). In brief, a total of 10 gastric cancer xenograft mice (27 g) randomly received an intravenous injection (tail vein) with Au–BSA–DOX–FA (10 mg/mL) or Au–BSA–DOX at a volume dose of 0.27 mL/27 g body weight. All mice were anesthetized with 250 μL of 5% chloral hydrate and then placed in a scanning holder. Prior to injection and at different times after the injection, CT scanning was carried out (tube voltage 80 kV; tube current 234 mA). The images were analyzed using a RadiAnt DICOM Viewer (Medixant, Poznan, Poland).

Histotoxicity analysis and in vivo antitumor activity studies

Histotoxicity analysis and antitumor activity were evaluated by histopathological analysis and by determination of the animal weight and tumor volume. In all, 30 gastric cancer xenograft mice were randomly and equally divided into three groups. Animals that received intravenous administration of PBS acted as the controls, while another 20 mice were injected intravenously with 3.0 mg/kg of free DOX and Au–BSA–DOX–FA nanocomposites (3.0 mg DOX/kg). The administration was performed once every 2 days until the 14th day. The body weight and tumor volumes were measured once every 3 days. The following equation was used to calculate the tumor volume:

$$\text{Tumor volume} = \text{length} \times \text{width}^2 \times 0.5$$

On the 21st day, animals were sacrificed using overdose anesthesia. Samples of the kidney, heart, liver, spleen and lung and also tumor tissues were dissected and fixed in 4% formalin. The samples were then dissected and embedded in paraffin, and 8 μm thick sections were prepared and stained with hematoxylin and eosin (H&E).

Statistical analysis

All data were given as the mean ± standard deviation of independent measurements and analyzed with the aid of SPSS software (version 16.0). Normally distributed data were considered to be statistically significant at $P<0.05$.

Results and discussion

Synthesis and characterization of Au–BSA–DOX–FA nanocomposites

In this research, Au–BSA NPs were initially prepared by reducing $HAuCl_4$ using ascorbic acid in the presence of BSA for one-pot synthesis, as schematically shown in Figure 2A. The whole synthetic process was fast, facile and eco-friendly (no toxic agents and organic solvents), which ensures the following compatibility. We previously reported that BSA was an excellent foaming and stabilizing agent that had been extensively used in the synthesis of nanomaterials.[41] After purification, these Au–BSA NPs were characterized in detail. First, the size distribution and morphology were validated using TEM and high-resolution transmission electron microscopy (HRTEM). As shown in Figure 2B, the as-prepared products were monodispersed and homogeneous, with a narrow size distribution centered around 50 nm, which matched with the criterion that NPs with a diameter of 10–200 nm permit long-term circulation and tumor targeting in vivo.[42] The magnified TEM image (Figure 2C) provided us with further insights into the morphological characteristics of NPs. The nanomaterials exhibited flowerlike 3D structures surrounded by many small individual NPs. Notably, these flowerlike 3D nanostructures displayed dark and bright contrast within the whole region of individual particles, revealing that the as-prepared products are organic/inorganic composites. It can be deduced that the dark component is an Au NP and the bright part is a BSA molecule. HRTEM further revealed that individual NPs had a single crystalline structure, with a lattice spacing of circa 0.23 (Figure 2D), which corresponded to the (111) Au facet. A thin layer (BSA) wrapped outside the lattice component was also observed, which contributes to the good stability and biocompatibility. The existence of a surface BSA coating was also indirectly confirmed by excellent colloidal stability in different solutions and pH values (Figure S1). Figure S2 shows the size distribution of the synthesized Au–BSA, Au–BSA–DOX and Au–BSA–DOX–FA NPs as measured by DLS. The mean diameter of Au–BSA, Au–BSA–DOX and Au–BSA–DOX–FA NPs was 51.4, 65.8 and 72.9 nm, respectively. It is interesting to note that the measured hydrodynamic size of the Au–BSA (Figure S2A) is much larger than that measured by TEM (48.8 nm, Figure 2C, inset). This is likely due to the fact that DLS measures the size of large aggregates or clusters of particles in an aqueous solution that may consist of many BSA, while TEM just measures single metal Au core alone.

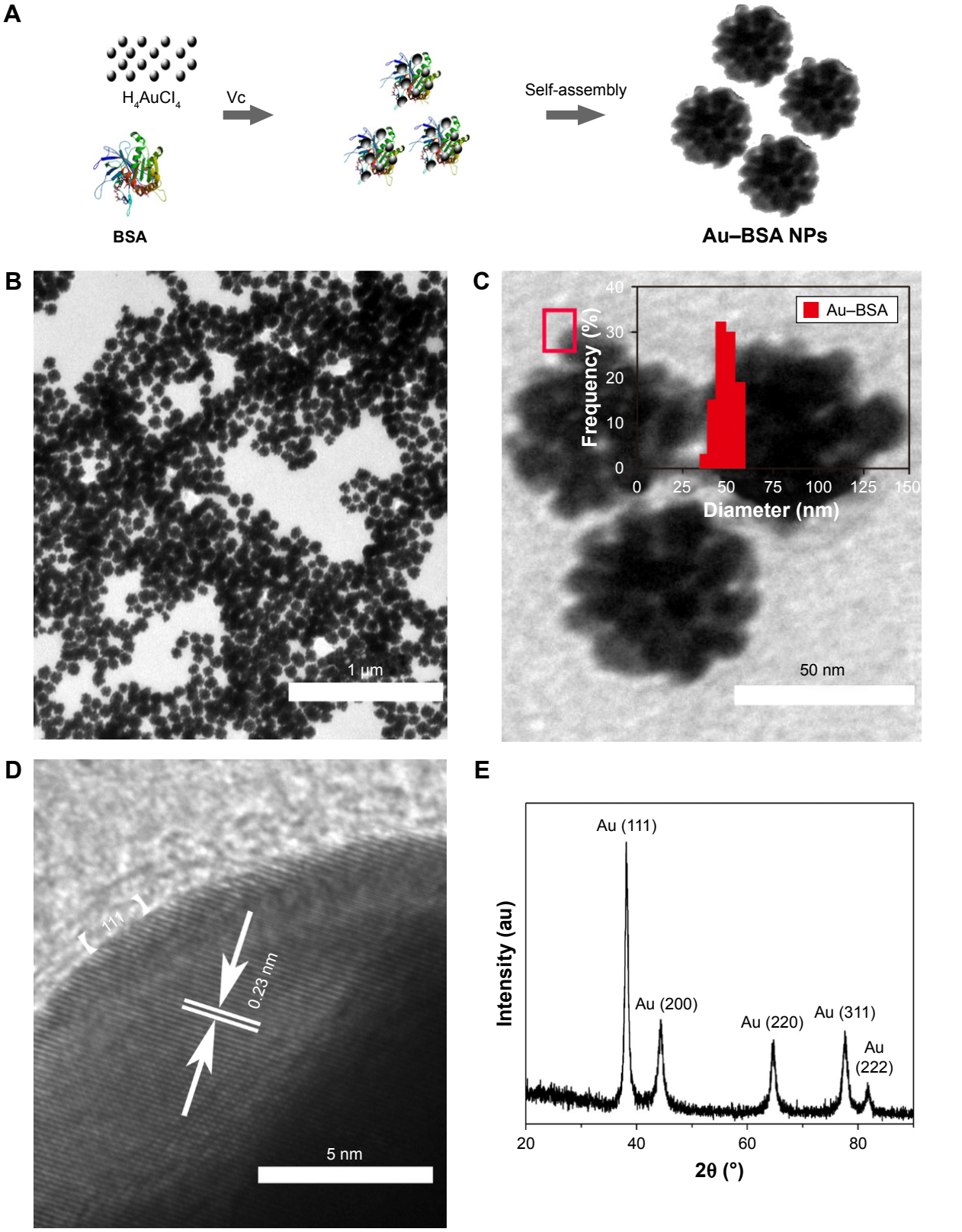

Figure 2 Design, fabrication and characterization of Au-BSA nanoparticles.
Notes: (**A**) Schematic of BSA-templated synthesis of Au–BSA NPs, (**B**) TEM images of Au–BSA NPs, (**C**) the magnified TEM images of Au–BSA NPs, (**D**) HRTEM images of Au–BSA NPs (arrows indicate lattice spacing) and (**E**) XRD analysis of Au–BSA NPs.
Abbreviations: BSA, bovine serum albumin; NPs, nanoparticles; TEM, transmission electron microscopy; HRTEM, high-resolution transmission electron microscopy; XRD, X-ray powder diffraction; au, gold; Vc, vitamin C.

X-ray powder diffraction (XRD) analysis (Figure 2E) showed five characteristic diffraction peaks at 38.2°, 44.3°, 64.7°, 77.7° and 82.0° corresponding to Au (111), Au (200), Au (220), Au (311) and Au (222) planes of face-centered cubic (fcc) Au, respectively, findings in good agreement with standards data published by the Joint Committee on Powder Diffraction Standards. No peaks corresponding to impurities were observed, suggesting that as-synthesized NPs were made entirely from pure crystalline gold. Moreover, the peak intensity corresponding to the (111) plane was greater than the other planes, indicating that (111) was the predominant orientation, which correlated with HRTEM measurements (Figure 2D). Together, Au was trapped within as-synthesized NPs as pure crystalline gold and thus offered a molecular basis for nanocomposites to be used as contrast agents.

In order to couple therapeutic agents and targeting molecules, it is important to identify functional chemical groups (e.g., –COOH or NH_2) on the surface of as-prepared products. Fourier transform infrared spectroscopy (FTIR) was employed as an efficient technique to determine the structure and formation of the Au NPs. As shown in Figure 3, the FTIR spectra of Au–BSA NPs displayed several characteristic peaks. The peak at 3,427 cm^{-1} was attributed to the stretching vibration of the O–H bond; the smaller peak at 2,375 cm^{-1} reflected the S–H bond vibration produced by stretching. The peaks that occurred at 1,637 and 1,385 cm^{-1} were attributed to the C=O stretching vibration and the $–CH_2$ group vibrations, respectively. The peaks at 613 cm^{-1} were ascribed to lysine in BSA. These findings indicated that BSA molecules are incorporated into the Au NPs, which is in good agreement with a previous study.[43] To confirm that the FA and DOX have been successfully immobilized, the FTIR spectra of Au–BSA–DOX and Au–BSA–DOX–FA were obtained (Figure 3B and C). The presence of several characteristic bands between 956 and 1,063 cm^{-1} was associated with the bond of FA. The presence of several bands in the range of 1,064–1,270 cm^{-1} was associated with the bond of DOX. These results further support the successful synthesis of the Au–BSA–DOX–FA nanocomposites.

Sufficient conjugation of therapeutic drugs and successful coupling of targeting agents plays a key role in building nanocomposites. UV–vis measurements were carried out to confirm the conjugation of DOX and FA molecules on Au–BSA NPs. As shown in Figure 4, the pure FA and DOX solution showed the characteristic absorption at 360 and 495 nm. The purified Au–BSA NPs absorption peak occurred at 280 nm, revealing that BSA molecules are involved in the formation of nanomaterials. In addition, the peaks at 580 nm showed a characteristic surface plasmon resonance band of Au NPs, which is consistent with the results of TEM observation. The characteristic absorption peaks of

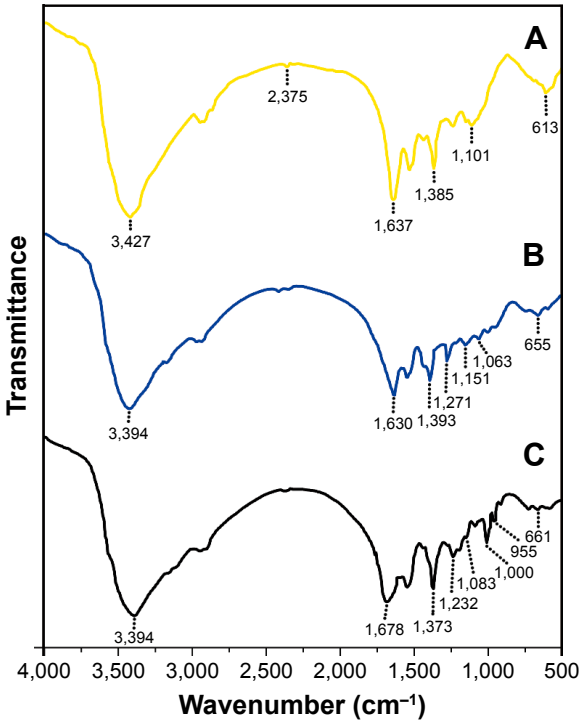

Figure 3 The FTIR spectra of Au–BSA (**A**), Au–BSA–DOX (**B**) and Au–BSA–DOX–FA (**C**).
Abbreviations: BSA, bovine serum albumin; DOX, doxorubicin; FA, folic acid; FR, folate receptor; FTIR, Fourier transform infrared spectroscopy.

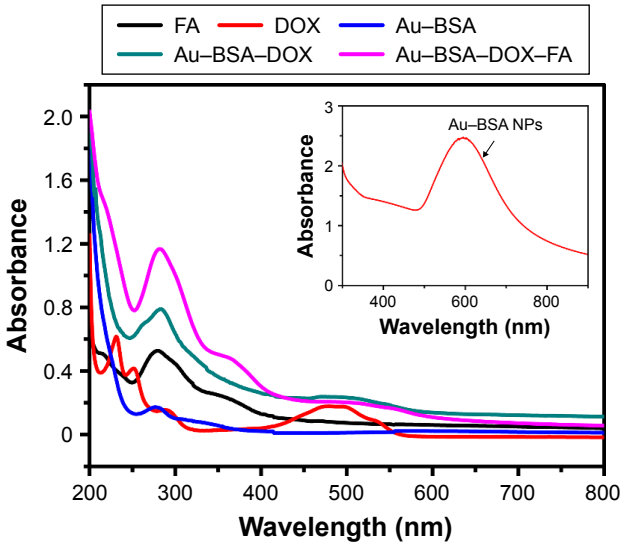

Figure 4 UV–vis spectroscopy of FA, DOX, Au–BSA, Au–BSA–DOX and Au–BSA–DOX–FA in distilled water.
Note: Inset: the UV–vis spectra of Au–BSA NPs at high concentrations.
Abbreviations: UV, ultraviolet; FA, folic acid; DOX, doxorubicin; BSA, bovine serum albumin; NPs, nanoparticles.

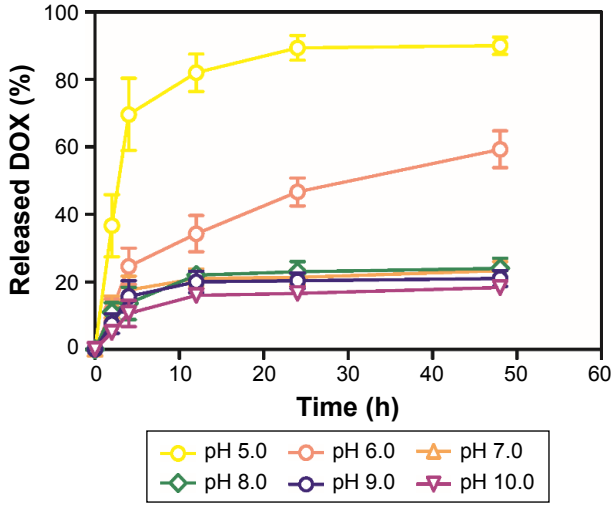

Figure 5 Effect of pH on DOX release from the Au–BSA–DOX–FA nanocomposites.
Abbreviations: DOX, doxorubicin; BSA, bovine serum albumin; FA, folic acid.

BSA, FA and DOX at 280, 360 and 495 nm, respectively, were detected in Au–BSA–DOX–FA nanocomposites, indicating the successful combination of DOX and FA on the surface of Au–BSA NPs.

pH-sensitive drug release ability and cytotoxicity

To achieve the pH sensitivity of the functional nanomaterials, *cis*-aconityl linker was introduced to bind DOX onto the Au–BSA NPs. The controlled release of DOX from Au–BSA–DOX–FA nanocomposites was investigated by quantifying DOX amounts in the presence of different pH media. The in vitro drug release profiles are shown in Figure 5. At pH 7.0 and 9.0, we found that the amount of DOX released from the nanocomposites reached ~20%. In contrast, at pH 5.0, the released amount of DOX was >90%, which is ~4.5-fold higher than the former. The rapid release of DOX from nanocomposites in acid condition could be attributed to the *cis*-aconityl linkage, which is more readily broken at pH <6. A previous study indicated that pH-sensitive release of DOX was dependent on the association of free carboxylic groups in an acidic environment.[22] *Cis*-transformation is also involved in catalyzing intramolecular hydrolysis of amide bonds. Overall, the release profiles of DOX from Au–BSA–DOX–FA nanocomposites indicate that they will be stable during circulation and drugs can be rapidly released in the acid tumor condition.[44,45]

Prior to identifying the anticancer properties of Au–BSA–DOX–FA nanocomposites, it was necessary to evaluate the original carrier Au–BSA NP cytotoxicity. Data in Figure 6 clearly show that the viability of both GES-1 and MGC-803 cells was not statistically influenced by Au–BSA NPs at concentrations ranging from 0 to 100 μg/mL. These findings suggested that Au–BSA NPs do not affect the proliferation of both malignant and normal cells.

The membrane-bound protein FR, which binds and transports folate with high affinity, has been proven to be aberrantly overexpressed in various malignant tumors to meet the requirements of rapidly dividing cancer cells.[46] Thus, the expression of FR in human mucosa GES-1 and gastric cancer MGC-803 cells was quantified in order to identify whether or not these cells could be utilized to validate specific targeting and the anticancer properties of Au–BSA–DOX–FA nanocomposites. We found that relative mRNA expressions of FR in MGC-803 were statistically higher than those in GES-1 cells (10±3.10 vs 1±0.27, P=0.011; Figure S3), meaning that

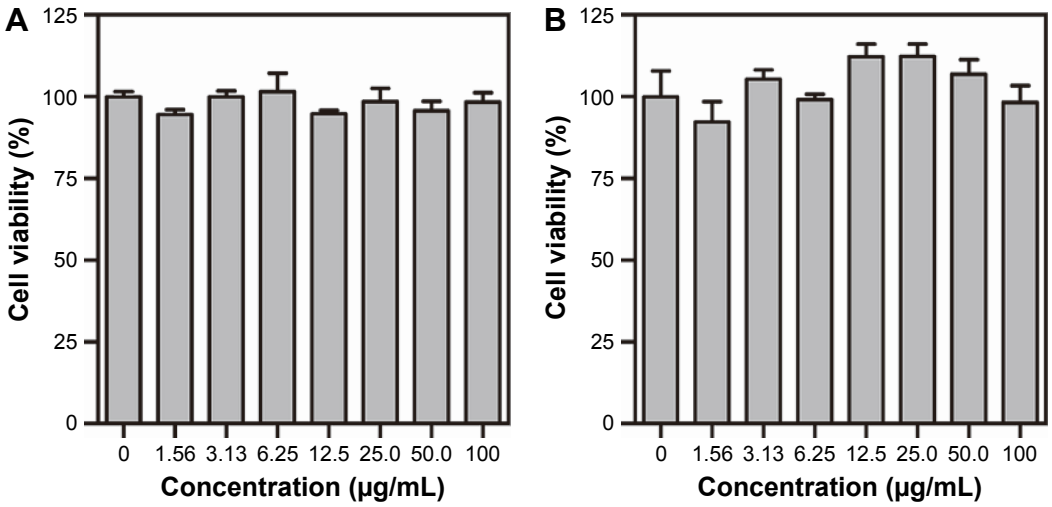

Figure 6 Cell viabilities of normal cells and cancer cells incubated with Au–BSA NPs.
Notes: (**A**) Human gastric mucosa GES-1 cells. (**B**) Human gastric cancer MGC-803 cells.
Abbreviations: BSA, bovine serum albumin; NPs, nanoparticles.

MGC-803 cells preferred to bind FA or Au–BSA–DOX–FA nanocomposites.[16]

In vitro anticancer activity

Taking into account the abovementioned promising results, we next explored the potential of Au–BSA–DOX–FA nanocomposites as anticancer agents and compared the effects with free DOX. DOX is an efficient DNA-interacting drug widely used in chemotherapy for the treatment of various cancers. Figure 7 summarizes the results obtained with free DOX and Au–BSA–DOX–FA nanocomposites. It is important to note that we ensured that the drug amount in free DOX is similar to that present in Au–BSA–DOX–FA nanocomposites. Regardless of whether MGC-803 or GES-1 was the system tested, the viability of cells showed a DOX concentration-dependent decrease. Compared with free DOX, the Au–BSA–DOX–FA nanocomposites exhibited a higher cell-inhibition rate to MGC-803 cells at various concentrations (Figure 7B). In contrast, the Au–BSA–DOX–FA nanocomposites did not exhibit a superior inhibition rate to GES-1 cells compared with free DOX; indeed, the inhibition rate was lower at various concentrations (Figure 7A). This means that the Au–BSA–DOX–FA nanocomposites possess selective therapeutic efficacy to FR-overexpressing tumor cells and a low cytotoxicity to normal cells.

In vivo targeting ability and CT imaging

As is well known, Au nanomaterials can be used as a type of novel CT contrast agents in tumor imaging, owing to their brilliant X-ray attenuation properties. To test the CT imaging and targeting ability of Au–BSA–DOX–FA, we chose human gastric cancer xenografted mice as the animal model. Figure 8A shows CT tumor images (dotted portion) before and after the intravenous administration of Au–BSA–DOX–FA nanocomposites or Au–BSA–DOX NPs.

Owing to the fine distinction of brightness, it was difficult to analyze the CT images of tumor sites by the naked eye. Therefore, we resorted to the manufacturer's standard display program. As shown in Figure 8B, the tumor CT imaging enhancements were further quantified by measuring the Hounsfield units (HUs) at different times. In general, the CT values of tumor tissues gradually increased after injection of Au–BSA–DOX–FA nanocomposites (targeted group) or Au–BSA–DOX NPs (non-targeted group). The CT values of tumor tissue increased significantly after injection compared to before injection in the non-targeted group. This enhancement may be ascribed to the enhanced permeability and retention (EPR) phenomenon, which allows for the passive accumulation of Au–BSA–DOX NPs in tumor tissues. Therefore, our results suggest that Au–BSA–DOX NPs will be very useful as contrast agents in X-ray CT imaging in vivo. It is noteworthy that the CT values of tumors in the target group injected with Au–BSA–DOX–FA nanocomposites were much greater than those of the non-targeted group 30 min after injection. This result indicated that Au–BSA–DOX–FA nanocomposites can target FR-overexpressing tumor tissue and result in the enhancement of CT attenuation.

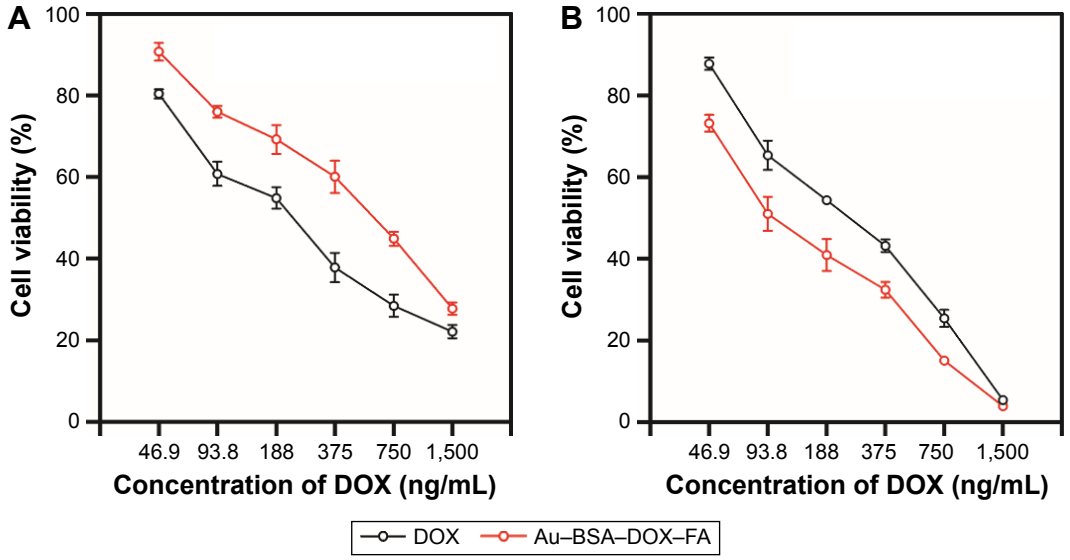

Figure 7 Cell viabilities of cancer and normal cells incubated with free DOX and Au–BSA–DOX–FA nanocomposites.
Notes: (**A**) Human gastric mucosa GES-1 cells. (**B**) Human gastric cancer MGC-803 cells.
Abbreviations: DOX, doxorubicin; BSA, bovine serum albumin; FA, folic acid.

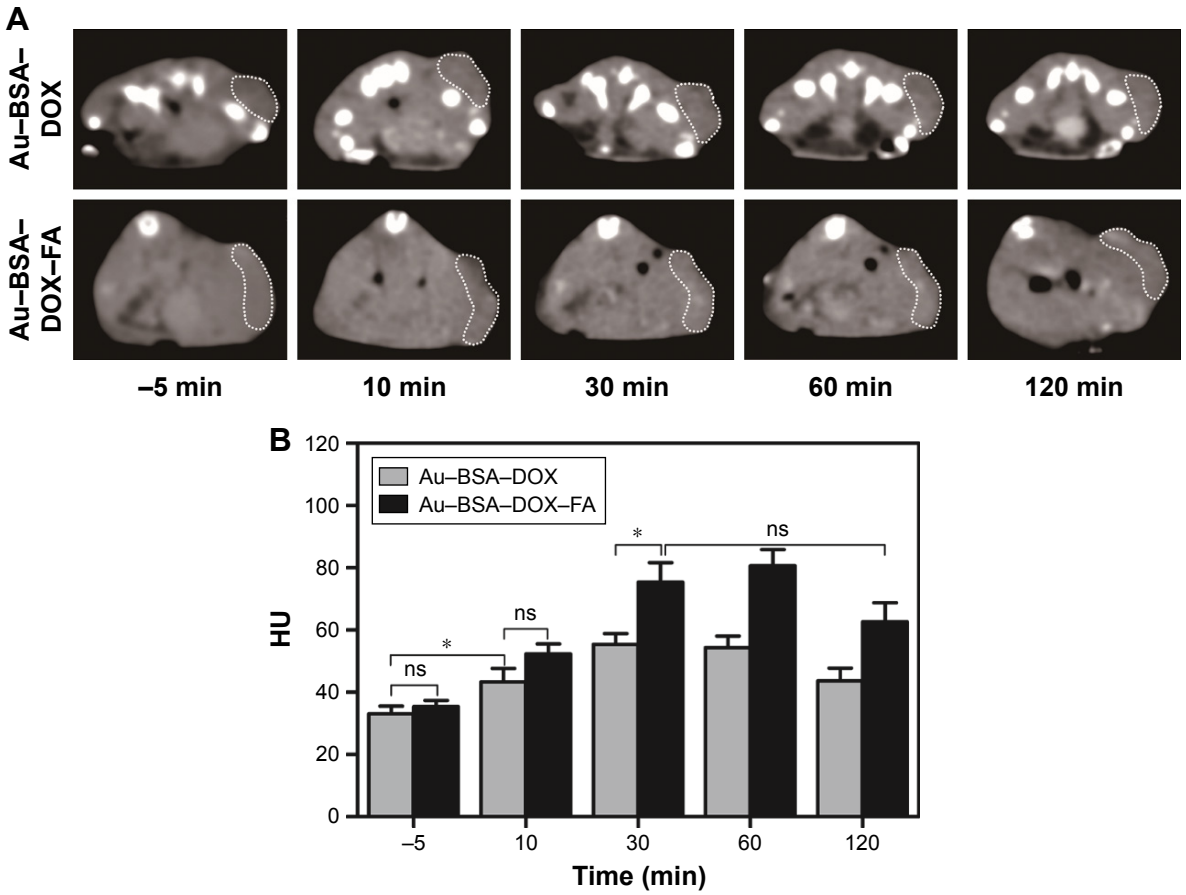

Figure 8 CT images (**A**) and values (**B**) of gastric cancer tissues in nude mice before (–5 min) and at different time points post injection of the Au–BSA–DOX–FA nanocomposites or Au–BSA–DOX NPs (n=5 per group).
Notes: The dotted dash indicates tumor (magnification 1:1). *$P \leq 0.05$.
Abbreviations: CT, computed tomography; BSA, bovine serum albumin; DOX, doxorubicin; FA, folic acid; NPs, nanoparticles; HU, Hounsfield unit; ns, not significant.

The highest CT value in tumor arose at 30 min postinjection, which was maintained for 60 min and then followed by a slight decrease at 120 min in the targeted group. Au–BSA–DOX–FA nanocomposites are durable X-ray contrast agents compared to the currently used iodine-based compounds.[10] Compared with iodine-based CT contrast agents, Au–BSA–DOX–FA nanocomposites are able to target specifically tumors and notably are retained for longer time periods.

Histotoxicity

To identify further whether Au–BSA–DOX–FA nanocomposites have histotoxicity, histopathological analysis was carried out. Free DOX caused obvious pathological changes in mice, including myocardial cell granular degeneration and the breakdown of hyaline casts in the tubules of the kidneys. Coupled DOX resulted in decreased histotoxicity and exhibited histostructures similar to those treated with PBS. Histopathological images of cancer tissues from mice treated with PBS were overgrown with malignant tumor cells. Free DOX led to a significant decrease in cancer cells, which was still higher than those treated with Au–BSA–DOX–FA nanocomposites bearing same DOX (Figure 9). The results indicated that Au–BSA–DOX–FA nanocomposites did not cause apparent toxicity in major organs, whereas free DOX produced severe toxicity in the heart and kidney. More importantly, Au–BSA–DOX–FA nanocomposites have stronger antitumor activity than free DOX. The results of in vivo experiments were consistent with those obtained in vitro (Figure 7). These advantages can in all probability be attributed to the Au–BSA–DOX–FA nanocomposites' target activity.

In vivo antitumor activity

Specific anticancer activity of Au–BSA–DOX–FA nanocomposites was also validated by determining the animal weight and tumor volume. During the experimental course, mice administrated with buffer gradually lost their body weight,

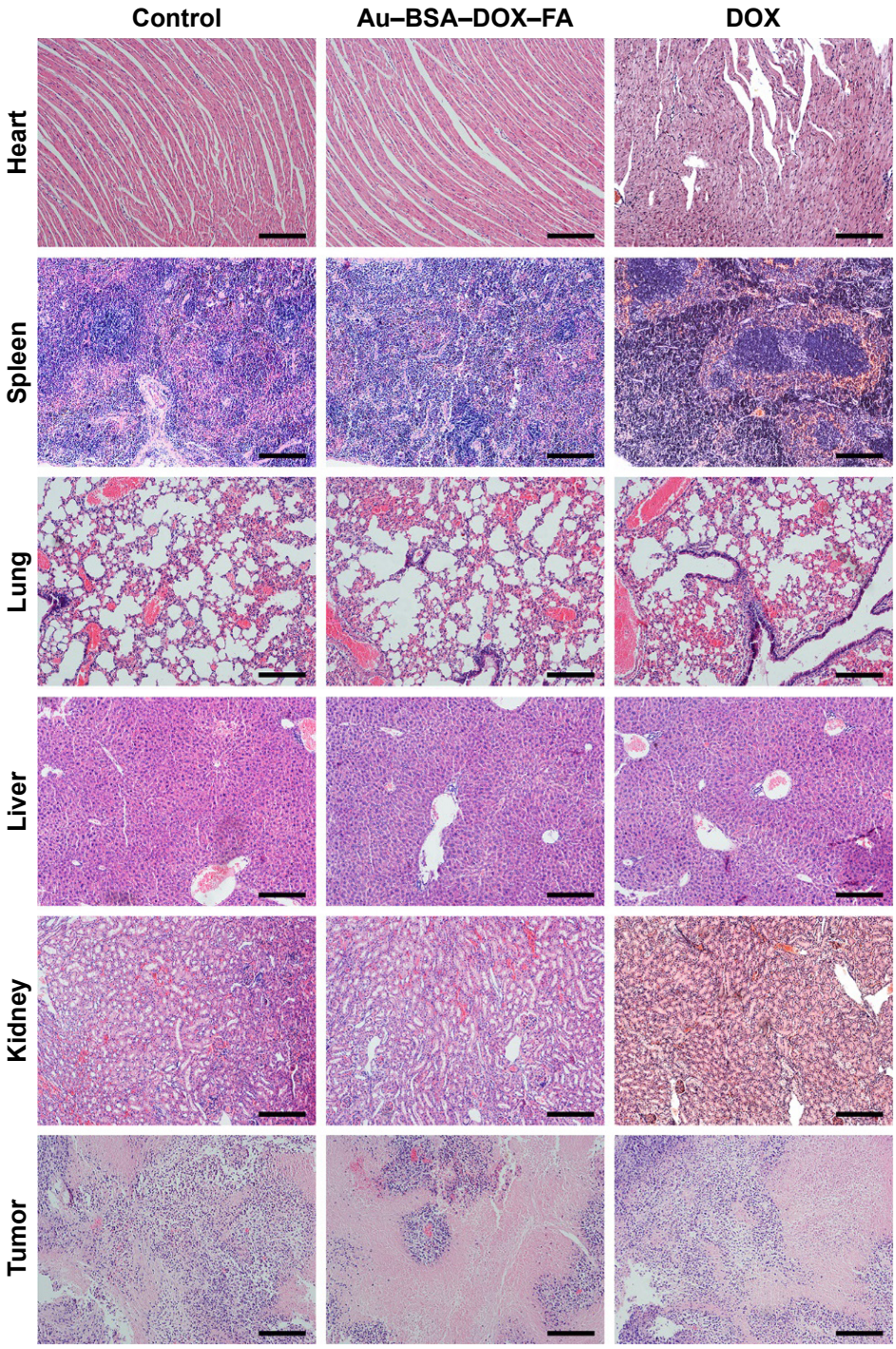

Figure 9 Histopathological analysis of main organs and cancer tissues from xenografted mice treated with PBS, Au–BSA–DOX–FA nanocomposites and free DOX (n=10 per group, scale bar =200 μm).
Abbreviations: PBS, phosphate-buffered saline; BSA, bovine serum albumin; DOX, doxorubicin; FA, folic acid.

ultimately up to 5.89% of their original weight. Similarly, body weight loss was also found in the other two groups of mice, who received free DOX (lost 12.91% of their original weight) or coupled DOX (lost 8.94% of their original weight; Figure 10). As a chemotherapeutic agent, DOX always produces serious adverse drug reactions such as nausea and vomiting, eventually leading to weight lost. By virtue of pH-sensitive release, Au–BSA–DOX–FA nanocomposites remain stable during circulation, thereby avoiding gastrointestinal reactions and weight loss.

As expected, administration of buffer resulted in a rapid development of gastric tumors, which exhibited an initial

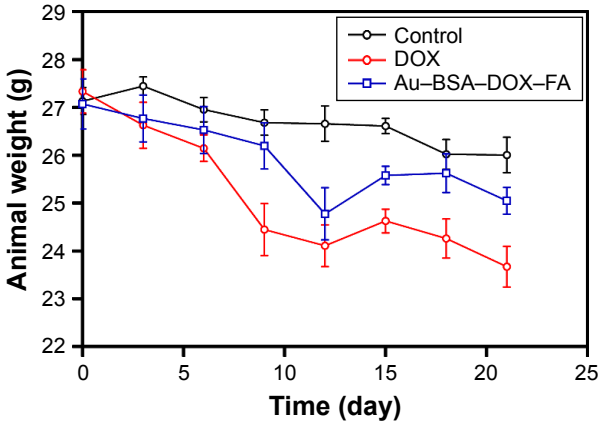

Figure 10 Animal weight of xenografted mice treated with PBS, Au–BSA–DOX–FA nanocomposites and free DOX (n=10 per group).
Abbreviations: PBS, phosphate-buffered saline; BSA, bovine serum albumin; DOX, doxorubicin; FA, folic acid.

0.11 cm^3 to an ultimate 0.99 cm^3 increase in tumor volume. In contrast, intravenous injection of free and coupled DOX showed significant inhibitory effects on cancer development, displaying an ultimate 0.37 and 0.25 cm^3 increase in tumor volumes, respectively. Although having comparable effects on tumor volume initially, the usage of coupled DOX caused significantly powerful inhibition of tumor volume from day 15, which was maintained thereafter (Figure 11).

Compared to free DOX, Au–BSA–DOX–FA showed no pathological changes, a more profound inhibition of cancer cell growth, a more significant decrease in tumor volumes and more obvious effects on animal weight. These findings suggested that Au–BSA–DOX–FA nanocomposites also simultaneously offer targeting therapy with less histotoxicity,

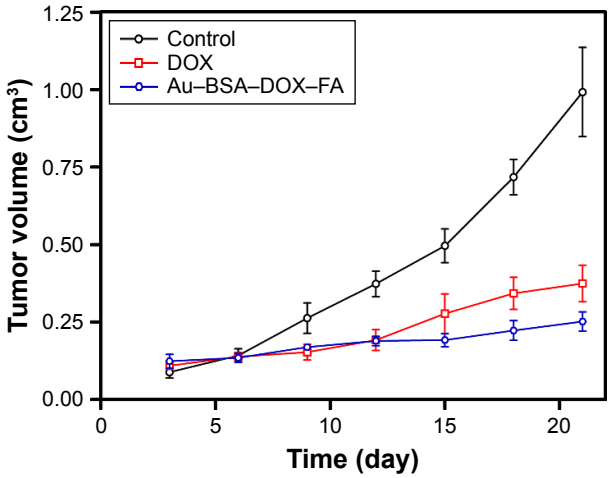

Figure 11 Tumor volume in xenografted mice treated with PBS, Au–BSA–DOX–FA nanocomposites and free DOX (n=10 per group).
Abbreviations: PBS, phosphate-buffered saline; BSA, bovine serum albumin; DOX, doxorubicin; FA, folic acid.

owing to FA-mediated endocytosis and the intracellular release of DOX as a consequence.[47]

Conclusion

An Au–BSA–DOX–FA nanocomposite has been successfully prepared and systematically characterized. It has the advantages of easy synthesis, good stability, convenient surface modification and excellent biocompatibility. More importantly, the multifunctional nanocomposite exhibits selective targeting, X-ray attenuation and pH-sensitive drug release activity. Therefore, it can enhance CT imaging and improve the targeting therapeutic efficacy of FR-overexpressing human gastric cancer. Taken together, our findings suggest that the Au–BSA–DOX–FA nanocomposite is a novel drug delivery carrier and a promising candidate for cancer theranostic applications.

Acknowledgments

This work was supported by the National Natural Science Foundation of China (Grant Nos 81472001, 81671839 and 31400851), the Natural Science Foundation of Shanghai (Grant Nos 15ZR1425300 and 15JC1490600), Funding of SJTU (Grant No YG2014MS01) and the Initial Foundation for Distinguished Scholars of Quanzhou Normal University.

Disclosure

The authors report no conflicts of interest in this work.

References

1. Sheng Z, Hu D, Zheng M, et al. Smart human serum albumin-indocyanine green nanoparticles generated by programmed assembly for dual-modal imaging-guided cancer synergistic phototherapy. *ACS Nano*. 2014; 8(12):12310–12322.
2. Song L, Guo Y, Roebuck D, et al. Terminal PEGylated DNA-Gold nanoparticle conjugates offering high resistance to nuclease degradation and efficient intracellular delivery of DNA binding agents. *ACS Appl Mater Interfaces*. 2015;7(33):18707–18716.
3. Sperling RA, Rivera Gil P, Zhang F, Zanella M, Parak WJ. Biological applications of gold nanoparticles. *Chem Soc Rev*. 2008;37(9):1896–1908.
4. Chen CT, Chen WJ, Liu CZ, Chang LY, Chen YC. Glutathione-bound gold nanoclusters for selective-binding and detection of glutathione S-transferase-fusion proteins from cell lysates. *Chem Commun (Camb)*. 2009;(48):7515–7517.
5. Bajaj A, Miranda OR, Kim IB, et al. Detection and differentiation of normal, cancerous, and metastatic cells using nanoparticle-polymer sensor arrays. *Proc Natl Acad Sci U S A*. 2009;106(27):10912–10916.
6. El-Sayed IH, Huang X, El-Sayed MA. Surface plasmon resonance scattering and absorption of anti-EGFR antibody conjugated gold nanoparticles in cancer diagnostics: applications in oral cancer. *Nano Lett*. 2005; 5(5):829–834.
7. Jiang S, Win KY, Liu S, Teng CP, Zheng Y, Han MY. Surface-functionalized nanoparticles for biosensing and imaging-guided therapeutics. *Nanoscale*. 2013;5(8):3127–3148.
8. Xiao Y, Hong H, Matson VZ, et al. Gold nanorods conjugated with doxorubicin and cRGD for combined anticancer drug delivery and PET imaging. *Theranostics*. 2012;2(8):757–768.

9. Chen G, Xie Y, Peltier R, et al. Peptide-decorated gold nanoparticles as functional nano-capping agent of mesoporous silica container for targeting drug delivery. *ACS Appl Mater Interfaces*. 2016;8(18):11204–11209.
10. Liu H, Wang H, Xu Y, et al. Lactobionic acid-modified dendrimer-entrapped gold nanoparticles for targeted computed tomography imaging of human hepatocellular carcinoma. *ACS Appl Mater Interfaces*. 2014;6(9):6944–6953.
11. Arvizo RR, Bhattacharyya S, Kudgus RA, Giri K, Bhattacharya R, Mukherjee P. Intrinsic therapeutic applications of noble metal nanoparticles: past, present and future. *Chem Soc Rev*. 2012;41(7):2943–2970.
12. Liu H, Wang H, Xu Y, et al. Synthesis of PEGylated low generation dendrimer-entrapped gold nanoparticles for CT imaging applications. *Nanoscale*. 2014;6(9):4521–4526.
13. Liu Y, Ashton JR, Moding EJ, et al. A plasmonic gold nanostar theranostic probe for in vivo tumor imaging and photothermal therapy. *Theranostics*. 2015;5(9):946–960.
14. Ashton JR, Clark DP, Moding EJ, et al. Dual-energy micro-CT functional imaging of primary lung cancer in mice using gold and iodine nanoparticle contrast agents: a validation study. *PLoS One*. 2014;9(2):e88129.
15. Wang Z, Huang P, Jacobson O, et al. Biomineralization-inspired synthesis of copper sulfide-ferritin nanocages as cancer theranostics. *ACS Nano*. 2016;10(3):3453–3460.
16. Chen H, Li S, Li B, et al. Folate-modified gold nanoclusters as near-infrared fluorescent probes for tumor imaging and therapy. *Nanoscale*. 2012;4(19):6050–6064.
17. Murawala P, Tirmale A, Shiras A, Prasad BL. In situ synthesized BSA capped gold nanoparticles: effective carrier of anticancer drug methotrexate to MCF-7 breast cancer cells. *Mater Sci Eng C Mater Biol Appl*. 2014;34:158–167.
18. Ding C, Tian Y. Gold nanocluster-based fluorescence biosensor for targeted imaging in cancer cells and ratiometric determination of intracellular pH. *Biosens Bioelectron*. 2015;65:183–190.
19. Rana S, Bajaj A, Mout R, Rotello VM. Monolayer coated gold nanoparticles for delivery applications. *Adv Drug Deliv Rev*. 2012;64(2):200–216.
20. Elzoghby AO, Samy WM, Elgindy NA. Protein-based nanocarriers as promising drug and gene delivery systems. *J Control Release*. 2012;161(1):38–49.
21. Meng F, Zhong Y, Cheng R, Deng C, Zhong Z. pH-sensitive polymeric nanoparticles for tumor-targeting doxorubicin delivery: concept and recent advances. *Nanomedicine (Lond)*. 2014;9(3):487–499.
22. Du C, Deng D, Shan L, et al. A pH-sensitive doxorubicin prodrug based on folate-conjugated BSA for tumor-targeted drug delivery. *Biomaterials*. 2013;34(12):3087–3097.
23. Lee N, Choi SH, Hyeon T. Nano-sized CT contrast agents. *Adv Mater*. 2013;25(19):2641–2660.
24. Lusic H, Grinstaff MW. X-ray-computed tomography contrast agents. *Chem Rev*. 2013;113(3):1641–1666.
25. Peng C, Zheng L, Chen Q, et al. PEGylated dendrimer-entrapped gold nanoparticles for in vivo blood pool and tumor imaging by computed tomography. *Biomaterials*. 2012;33(4):1107–1119.
26. Reuveni T, Motiei M, Romman Z, Popovtzer A, Popovtzer R. Targeted gold nanoparticles enable molecular CT imaging of cancer: an in vivo study. *Int J Nanomedicine*. 2011;6:2859–2864.
27. Cole LE, Vargo-Gogola T, Roeder RK. Bisphosphonate-functionalized gold nanoparticles for contrast-enhanced X-ray detection of breast microcalcifications. *Biomaterials*. 2014;35(7):2312–2321.
28. Hallouard F, Anton N, Choquet P, Constantinesco A, Vandamme T. Iodinated blood pool contrast media for preclinical X-ray imaging applications – a review. *Biomaterials*. 2010;31(24):6249–6268.
29. Kim JY, Ryu JH, Schellingerhout D, et al. Direct imaging of cerebral thromboemboli using computed tomography and fibrin-targeted gold nanoparticles. *Theranostics*. 2015;5(10):1098–1114.
30. Popovtzer R, Agrawal A, Kotov NA, et al. Targeted gold nanoparticles enable molecular CT imaging of cancer. *Nano Lett*. 2008;8(12):4593–4596.
31. Al Zaki A, Joh D, Cheng Z, et al. Gold-loaded polymeric micelles for computed tomography-guided radiation therapy treatment and radiosensitization. *ACS Nano*. 2014;8(1):104–112.
32. Coughlin AJ, Ananta JS, Deng N, Larina IV, Peruzzi P, West JL. Gadolinium-conjugated gold nanoshells for multimodal diagnostic imaging and photothermal cancer therapy. *Small*. 2014;10(3):556–565.
33. Kim D, Park S, Lee JH, Jeong YY, Jon S. Antibiofouling polymer-coated gold nanoparticles as a contrast agent for in vivo X-ray computed tomography imaging. *J Am Chem Soc*. 2007;129(24):7661–7665.
34. Wang H, Zheng L, Peng C, Shen M, Shi X, Zhang G. Folic acid-modified dendrimer-entrapped gold nanoparticles as nanoprobes for targeted CT imaging of human lung adenocarcinoma. *Biomaterials*. 2013;34(2):470–480.
35. Eck W, Nicholson AI, Zentgraf H, Semmler W, Bartling S. Anti-CD4-targeted gold nanoparticles induce specific contrast enhancement of peripheral lymph nodes in X-ray computed tomography of live mice. *Nano Lett*. 2010;10(7):2318–2322.
36. Mahmoudi M, Serpooshan V, Laurent S. Engineered nanoparticles for biomolecular imaging. *Nanoscale*. 2011;3(8):3007–3026.
37. Kim D, Jeong YY, Jon S. A drug-loaded aptamer-gold nanoparticle bioconjugate for combined CT imaging and therapy of prostate cancer. *ACS Nano*. 2010;4(7):3689–3696.
38. Hu D, Sheng Z, Fang S, et al. Folate receptor-targeting gold nanoclusters as fluorescence enzyme mimetic nanoprobes for tumor molecular colocalization diagnosis. *Theranostics*. 2014;4(2):142–153.
39. Qiao J, Mu X, Qi L, Deng J, Mao L. Folic acid-functionalized fluorescent gold nanoclusters with polymers as linkers for cancer cell imaging. *Chem Commun (Camb)*. 2013;49(73):8030–8032.
40. Huang P, Bao L, Zhang C, et al. Folic acid-conjugated silica-modified gold nanorods for X-ray/CT imaging-guided dual-mode radiation and photo-thermal therapy. *Biomaterials*. 2011;32(36):9796–9809.
41. Huang J, Lin L, Sun D, Chen H, Yang D, Li Q. Bio-inspired synthesis of metal nanomaterials and applications. *Chem Soc Rev*. 2015;44(17):6330–6374.
42. Niikura K, Iyo N, Matsuo Y, Mitomo H, Ijiro K. Sub-100 nm gold nanoparticle vesicles as a drug delivery carrier enabling rapid drug release upon light irradiation. *ACS Appl Mater Interfaces*. 2013;5(9):3900–3907.
43. Wang X, Yang DP, Huang P, et al. Hierarchically assembled Au microspheres and sea urchin-like architectures: formation mechanism and SERS study. *Nanoscale*. 2012;4(24):7766–7772.
44. Koshkaryev A, Sawant R, Deshpande M, Torchilin V. Immunoconjugates and long circulating systems: origins, current state of the art and future directions. *Adv Drug Deliv Rev*. 2013;65(1):24–35.
45. Zhang XQ, Xu X, Bertrand N, Pridgen E, Swami A, Farokhzad OC. Interactions of nanomaterials and biological systems: implications to personalized nanomedicine. *Adv Drug Deliv Rev*. 2012;64(13):1363–1384.
46. Kelemen LE. The role of folate receptor alpha in cancer development, progression and treatment: cause, consequence or innocent bystander? *Int J Cancer*. 2006;119(2):243–250.
47. Lin J, Zhou Z, Li Z, et al. Biomimetic one-pot synthesis of gold nanoclusters/nanoparticles for targeted tumor cellular dual-modality imaging. *Nanoscale Res Lett*. 2013;8(1):170.

Supplementary materials

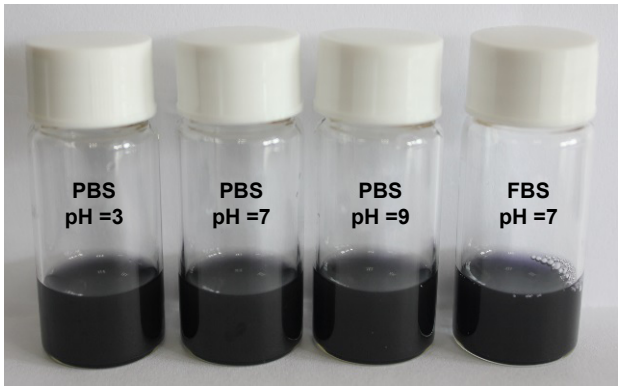

Figure S1 Photograph of Au–BSA NPs dispersed in different solutions (PBS and FBS) at various pH values (from left to right: pH =3, 7, 9 PBS and 7 FBS).
Abbreviations: BSA, bovine serum albumin; NPs, nanoparticles; PBS, phosphate-buffered saline; FBS, fetal bovine serum.

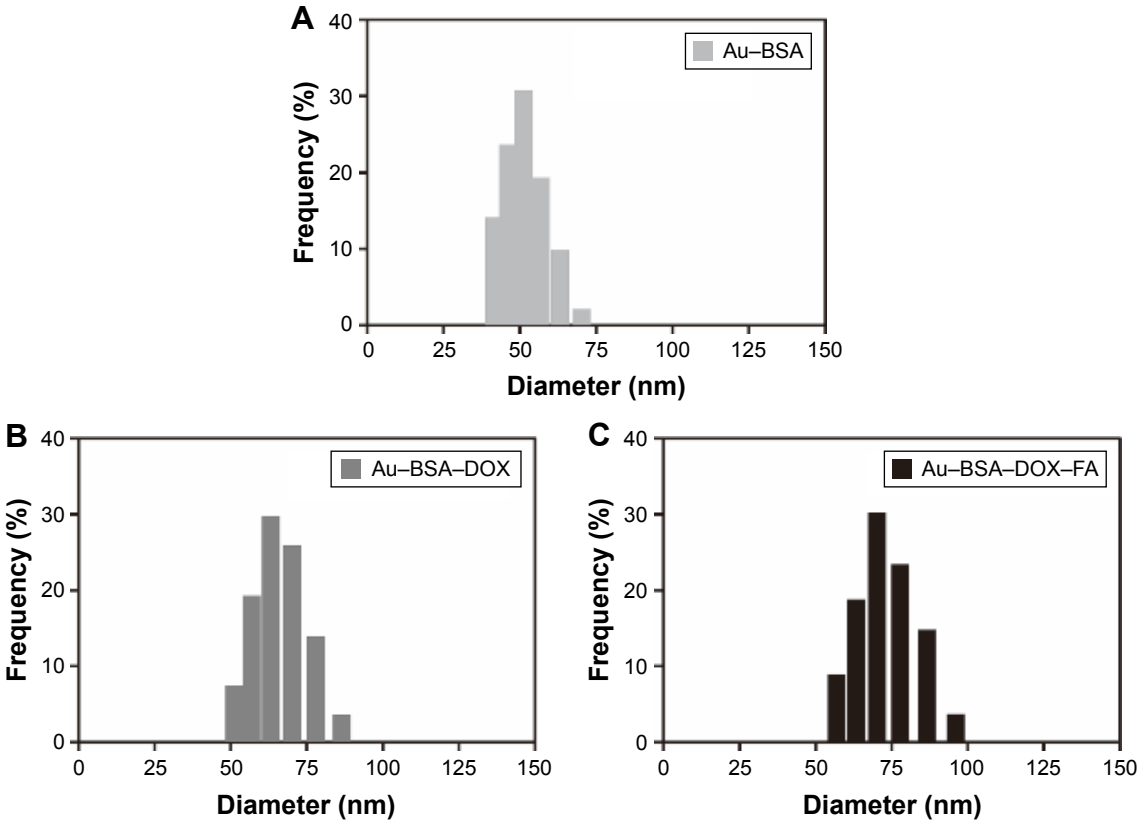

Figure S2 Hydrodynamic size distribution of (**A**) Au–BSA, (**B**) Au–BSA–DOX and (**C**) Au–BSA–DOX–FA.
Abbreviations: BSA, bovine serum albumin; DOX, doxorubicin; FA, folic acid.

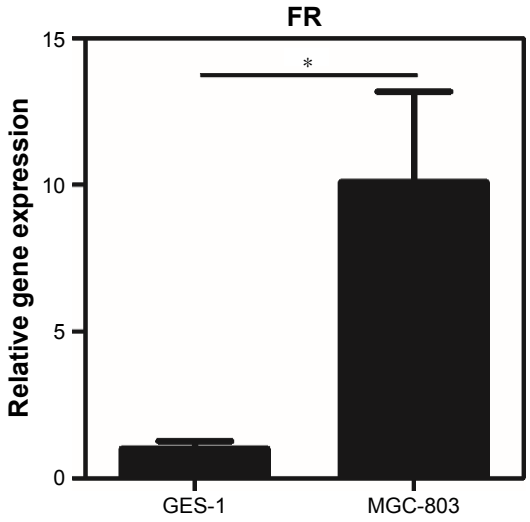

Figure S3 Expression of FR in MGC-803 and GES-1 cell lines analyzed by qRT-PCR.
Note: Each sample was tested in triplicate (n=3 per group). *$P \leq 0.05$.
Abbreviations: FR, folate receptor; qRT-PCR, quantitative reverse transcription polymerase chain reaction.